PAPER

Check for updates

Exploring rare earth elements in coalmine overburden: nanoscale insights from FESEM, TEM and XPS analysis

Binud Attry,[ab] K. S. V. Subramanyam,[c] Virendra M. Tiwari[ab] and Binoy K. Saikia [iD] *[ab]

Rare earth elements and yttrium (REY) are critical for various advanced technologies, particularly in electronics, and play a vital role in the economic growth of any country. Coal and its by-products could be potential precursors of these commodities and other natural resources. While coal and coal fly ash have been assessed for their REY content, the coal mine overburden (OB) or waste remains unexplored as a potential source of rare earth elements. The coal and coalmine OB samples of the Makum coalfield from the Northeastern region (NER) of India are examined and found to be promising sources of REY. This study presents the existence, distribution, and depositional conditions of REY in the coal and coalmine OB using various advanced analytical techniques, such as nanoscale morphology, Field Emission Scanning Electron Microscopy (FE-SEM), and High-Resolution Transmission Electron Microscopy (HR-TEM) to provide light on the geochemical behaviour and potential commercial viability of REY. The average value of REY in the study area is 167.66 mg kg^{-1} on a whole sample basis, in which the mean light (LREY) to heavy (HREY) ratio is 37.67. The average values of the europium anomaly (δEu), cerium anomaly (δCe), and Gadolinium anomaly (δGd) are 3.20, 0.71, and 5.30, respectively. The coal-forming conditions are characterized by slightly oxidizing and highly reducing environments, dominated by M-type enrichment, which are favourable for the weathering process. These conditions, marked by the absence of anaerobic microbial activity, facilitated the preservation of organic matter. Thus, the OB and coal deposits in this region present an opportunity for further exploration and assessment regarding the potential future recovery of REY.

Introduction

Coal and accompanying coalmine overburden (OB) contain numerous valuable elements. Such elements significantly contribute to forming the composition and structure of coal originating from ancient vegetative matter. However, post-depositional processes also account for the structure and metamorphism of coal, including heavy and rare earth elements and yttrium (REYs).[1,2] Large coal deposits are located in the Permian Gondwana formations of peninsular India and the Eocene to Oligocene strata (40–55 million years) from the NER.[3,4] According to the National Coal Inventory of 2023, of the Geological Survey of India (GSI), India's total projected coal resource is 378.21 billion tonnes as of 01.04.2023.[5–7] About 1739.37 million tonnes of coal deposits are found in the NER, primarily in the states of Assam, Arunachal Pradesh, Nagaland, Meghalaya, and Sikkim state, as per the coal inventory of India

reported by GSI as of 01.04.2021.[7] The coal mining activity also produces a large volume of mine leftovers containing rock, shale, and different types of soil, along with minerals and potentially hazardous elements (PHEs)[8,9] These coalmine left-overs, are called coalmine overburden (OB). This OB has not been scientifically explored for the presence of valuable elements, including REYs. Another frequent consequence of mining operations is the generation of acid mine drainage (AMD), which poses a serious environmental risk due to its highly acidic water and high concentrations of metals and metalloids. When sulfur-bearing rocks, such as pyrite found in coal and coalmine OB, are exposed to water and oxygen during mining operations, it generates AMD. This acidic water then seeps into the surrounding environment, leading to the release of potentially hazardous elements.[1,4,10–12] Makum coalfield (Margherita) is one of the active coalfields in Northeast India, producing high-sulfur Tertiary coal feedstock for the country. Because of its sulfur contents, the mining process generates AMD, resulting in acidic water.[13,14] However, the geochemical properties of the OB and AMD waters of this coalfield have not been explored, particularly regarding REY contents[14] and also there is a lack of REY potential data of coalmine OB as per our best-of-literature survey.

[a]CSIR-North East Institute of Science & Technology, Jorhat 785006, Assam, India. E-mail: bksaikia@neist.res.in; bksaikia@gmail.com

[b]Academy of Scientific & Innovative Research (AcSIR), Ghaziabad 201002, India

[c]CSIR – National Geophysical Research Institute, Uppal Road, Hyderabad 500007, India

Rare earth elements (REYs) denote a series of seventeen chemically and physically similar elements that occur together in the periodic table. They are consist of yttrium (Y), scandium (Sc), and the lanthanides: lanthanum (La), cerium (Ce), praseodymium (Pr), neodymium (Nd), promethium (Pm), samarium (Sm), europium (Eu), gadolinium (Gd), terbium (Tb), dysprosium (Dy), holmium (Ho), erbium (Er), thulium (Tm), ytterbium (Yb), and lutetium (Lu). The lanthanides from La to Lu are collectively known as the rare earth elements (REEs). Along with yttrium and scandium, they are jointly known as rare earth elements and yttrium (REY) as classified by the International Union of Pure and Applied Chemistry (IUPAC).[15–18] It is also sub-classified as light rare earth elements (LREEs: La to Eu), middle rare earth elements (MREEs: Gd to Ho), and heavy rare earth elements (HREEs: Er to Lu) and REYs can also be categorized based on their relationship of supply and demand into three types: critical (Nd, Eu, Tb, Dy, Y, and Er), non-critical (La, Pr, Sm, and Gd), and excessive (Ce, Ho, Tm, Yb, and Lu).[16] REYs are abundant in the earth's crust, hosted by the majority of the minerals.[19–21] Because these elements have many similar properties, they are usually encountered in the same geologic deposits together, so they are characterized by a few unique but comparable physicochemical properties.[16,22] It is to be noted that REYs are commonly regarded as the resources of the future due to their growing application in high-tech and other environmentally friendly sectors.[15,21,23] Due to their strategic significance and the anticipated discrepancy between their supply and demand in the future, REYs are categorized as "critical minerals" in the majority of countries like the United States of America (USA), the European Union (EU), etc.[23–26] In recent times, factors including scarcity, diversity, availability, and substitutability have been linked to the supply and demand of different commodities, and in light of these criteria, REYs have been designated as crucial components of strategic importance.

India occupies the fifth position in REY reserves and the sixth position in REY production.[27] Beach sands along India's eastern and western beaches are the primary sources of the country's REYs production.[28] Given that 29 of the 527 carbonatite occurrences of REY known worldwide have occurred in India,[29,30] and has a sizable latent potential for carbonatite-related REY deposits. However, other possible sources, including, NER coal and coalmine OB, which has not been attempted so far. Due to the huge applicability of REY in the technological segment to produce innovative industrial resources, such as superconductors, lasers, magnets, optical fibers, turbines, batteries, catalysts, and aerospace alloys, etc.,[16,25,31] finding alternate sources of the REY recovery is a topic of high relevance recently.

Therefore, this study attempts to comprehensively understand the geochemistry of REY along with the trace elements in coal, coalmine OB, and AMD water samples from the study area. The behavior of the REY will provide information about the accumulation and, deposition of the elements in the nearby areas of the Makum coalfield. Also, special importance has been given to the evaluation of the REY in coalmine OB samples as the literature is very much scanty for REY source analysis. Thus, despite their worldwide importance, the distribution of REY in coalmine OB has not been evaluated scientifically in India. The objective of the study is to understand the distribution, quantification, and geochemical behavior of REY in high-sulfur coal and associated coalmine OB samples from Makum coalfield in Northeast India, which is reported for the first time in this current study. This work will also provide insights into the mutual geochemical relationship among the geochemical parameters and different coal and coalmine OB samples. This study also contributes valuable baseline geochemical data that can promote environmentally responsible mining practices and enhance our understanding of the complex depositional environment. To the best of our knowledge, no prior research has used Field emission scanning electron microscopy (FE-SEM) and X-ray photoelectron spectroscopy (XPS) to characterize REY in coal and OB samples from NER. Combining high-resolution morphological imaging and surface-sensitive chemical analysis, this innovative method thoroughly comprehends the nanoscale study of REY. Additionally, cerium (Ce) and europium (Eu) are redox-sensitive rare earth elements (REEs) and are good indicators of sedimentary environments, particularly redox conditions. Their presence in coal and overburden (OB) is controlled primarily by fluctuations in oxidation–reduction conditions, which are reflected in some geochemical parameters such as δCe and δEu anomalies. Therefore, studies on the Eu and Ce anomalies, their partitioning behavior, and interpretations are very much suggestive for making better interpretations, using elemental geochemistry such as REY and trace elements.

Geology of the study area

Makum coalfield is situated in the Tinsukia district of Assam, lying between 27°15′ to 27°25′N latitude and 95°40′ to 95°50′E longitude towards, the westernmost side of the Patkai range in the Northeast Region of India.[3,4,32,33] The other coalfields of Assam, Arunachal Pradesh, and Nagaland states in the NER are spread out over a straight overthrust chain called the "belt of Schuppen," where Tertiary formations have folded and scattered into several thrust slices.[34] Several viable seams in the Oligocene Tikak Parbat Formation—the highest component of the Barail Group—provide coal for the Makum coalfield, this coalfield generates a huge amount of coalmine OB due to open-cast mining.[34]

Open-cast mining produces huge amounts of waste rock, soil, and minerals, known as overburden (OB).[10] The Indian Bureau of Mines has reported that 755 440 hectares are covered by mining leases in India, and approximately 5% (37 772 ha) are mined.[12] During 2001–2002, 1870 million tonnes of OB were excavated to produce 623 Mt of coal.[12] Mining 250 Mt of coal produces about 1000 million cubic meters of OB, resulting in the annual loss of 60 km² of land and using 75 km² for dumping outside the pit.[12]

Sampling program

The coal (BAC1, BAC2, BAC3, BAC4, and BAC5) and OB (BOB1, BOB2, BOB3, and BOB4) samples were collected from the active Tirap open-cast mining sites. The AMD water samples (AMD1, SW1, KM1, MW1) were collected from the source point and the affected nearby area of Tirap collieries of Makum coalfield.
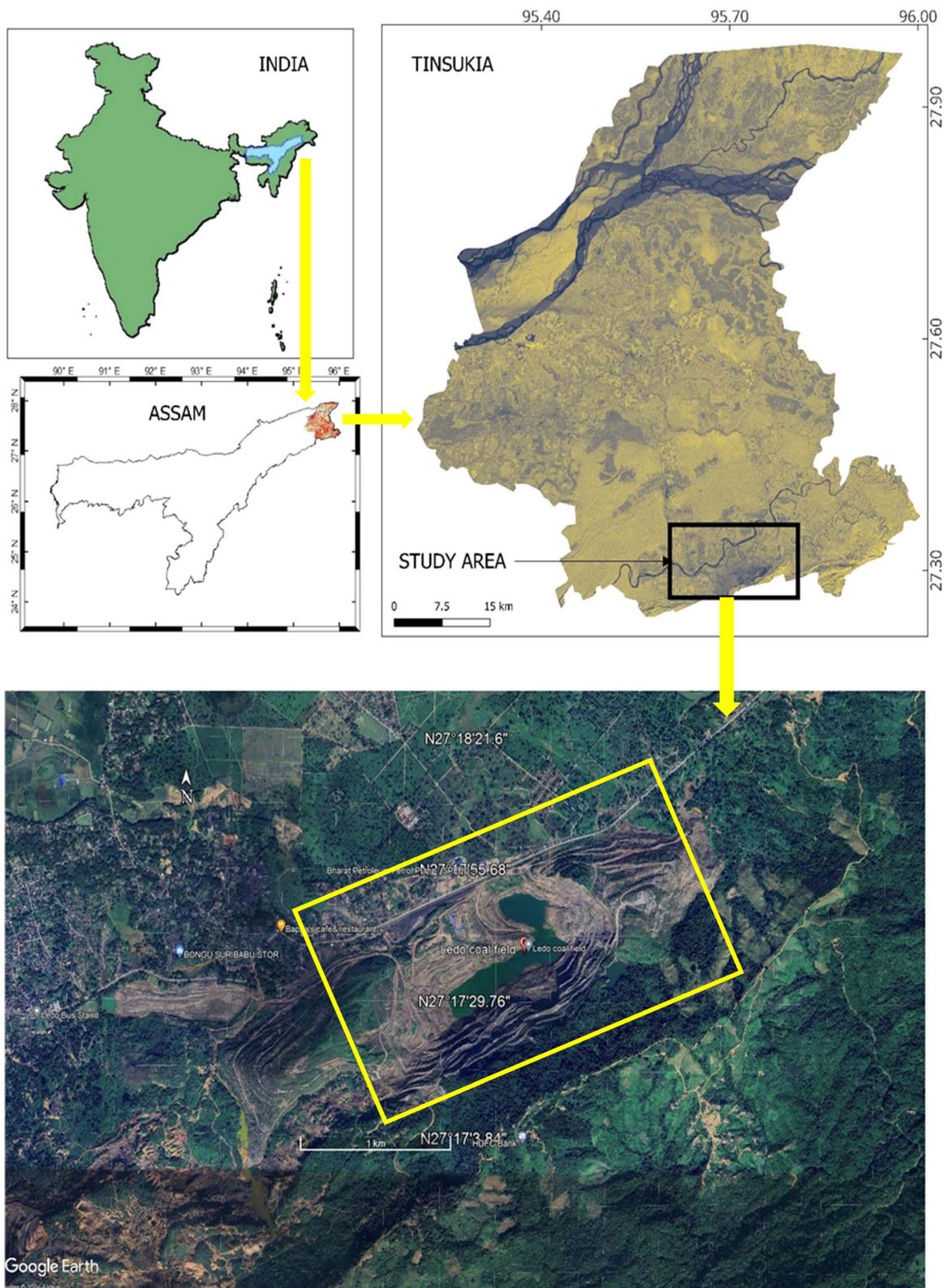
Fig. 1 Study area map of the Makum coalfield mining area in Assam, Northeast India.

The available standard procedures (ASTM 2020)[35] and (APHA 2020)[36,37] were applied to collect coal, OB, and water samples. The study area map generated by using QGIS (version: 3.30.2) and Google Earth Pro software is illustrated in Fig. 1.

Sample preparation

The collected coal and OB samples were air and sun-dried. Then, they were crushed and sieved to 212μ sizes using

© 2025 The Author(s). Published by the Royal Society of Chemistry

standard methods prescribed by ASTM.[35] The AMD water samples were filtered through a 0.45 μm syringe filter and kept in the refrigerator at 4 °C for further analysis.

Proximate analysis of coal and OB samples

The coal and OB samples were analysed to determine their physicochemical properties, including proximate (Method; ASTM D 7582-15) and total sulfur contents (Method: ASTM D4239 18). The samples were proximate analysed using a thermogravimetric analyser (Model: 117512122; Eltra Thermostep), and the total sulfur content was determined using a Sulphur Analyzer (Model: S-144DR; Leco Corporation, USA).

Elemental analysis by inductively coupled plasma mass spectrometry (ICP-MS)

The elemental contents including heavy metal and REY in the Coal, OB, and AMD water samples were quantified using ICP-MS (Model: Agilent 7850-SG22461707). Coal and OB samples were first digested in a microwave digestion system (Ethos Easy; Milestone Advance). Briefly, 50 mg of each coal and OB sample were mixed with 8 mL HNO_3 (65%, EMPLURA grade, Merck) followed by 1 mL H_2O_2 (HPLC grade, Molychem) and taken in the microwave digestion system. The Certified Reference Materials (Certipure® Reference Materials; Lot No. HC32534392) and CRM (CPAchem; Lot No. 860673) were used as standards and calibration of Heavy and REY, respectively, during ICPMS analysis.

X-ray photoelectron spectroscopy (XPS) analysis

To have insights into the elemental composition, oxidation states, molecular bonding environment, enable an understanding of surface chemistry, and the nature of chemical bonds present in the coal and coalmine OB samples, X-ray photoelectron spectroscopy (XPS) was performed in a Thermo-Scientific ESCALAB Xi+ spectrometer using a monochromatic Al Kα X-ray source (1486.6 eV) and a spherical energy analyser that functions in the constant analyser energy (CAE) mode using the electromagnetic lens. The CAE for high-resolution spectrum is 50 eV and that for survey spectra is 100 eV. For the measurement, a spectrum of 0–1300 eV was collected.

Field emission scanning electron microscope (FE-SEM) analysis

The outline of the minerals and the distribution of some specific elements on the raw coal and OB samples were studied using FE-SEM and an energy-dispersive X-ray spectrometer (EDS) (Genesis Apex 4) (Model No. ZEISS, SIGMA, Make: Carl ZEISS Microscopy, Germany). The SEM images were further improved using the "Image J" program (software version 1.47).

X-ray diffraction (XRD) analysis

The X-ray mineralogy was carried out in an X-ray diffractometer (Rigako, Ultima IV) and mineral phases were assessed following the previously reported literature.[38] The X-ray diffraction data of the materials were obtained using a target Cu Kα (1.54056 Å),

starting and stopping angles of 2° and 90°, step angle of 0.02°, and scanning rate of 1 °C min^{-1}.

Quality assurance and quality control (QA/QC)

Quality assurance and quality control (QA/QC) measures were implemented throughout all steps, from sample collection to analysis. New high-quality plastic zip bags were used to store the coal and OB samples during collection. The high-density polyethylene (HDPE) bottles and all the glassware used in the chemical analysis were dipped in 10% HNO_3 solution for 24 hours and then washed properly with deionized (DI) water. The blank was prepared and tested to ensure that the chemical used in the analysis was not contaminated in any way. Required standard solutions were prepared using the CRMs as mentioned earlier. During sample analysis, the procedural blank and standard were analysed and compared after every 5 samples to ensure the accuracy of the solvents and instrument. The element recovery rate was observed between 90 and 110% of the original value and the relative standard deviation was under 10%.

Result and discussions

Physico-chemical properties of coal, OB, and AMD water samples

The basic chemistry of the coal and OB samples were summarised in Table 1. It is seen that the average fixed carbon contents are different for coal and OB samples accounting for 51% and 10%, respectively. Similarly, volatile matter for coal was also higher than OB, however, ash content was higher for OB at an average of 70.79% compared to coal (7.65%), indicating the presence of significant inorganic contents in the OB. Coal resulted by the geochemical and biological disintegration of plant debris in swampy areas that form peat, which is then buried and transformed under pressure and heat during the diagenesis and coalification processes. As volatile chemicals are removed, these processes produce a denser, carbon-rich product with a higher fixed carbon content. On the other hand, sedimentation processes that do not entail substantial organic accumulation or carbon enrichment produce OB. Thus, coal seams with substantial levels of fixed carbon are created by

Table 1 Physico-chemical data of coal and OB samples (wt%; as received basis)^a

Sample	M	Ash	VM	FC	TS
BAC1	2.6525	3.0560	40.1005	54.1910	6.94
BAC2	3.4973	12.3934	35.6407	48.4686	3.74
BAC3	2.9643	3.3167	39.8099	53.9090	5.44
BAC4	3.9131	10.3124	36.7187	49.0559	3.90
BAC5	3.4934	9.1716	37.0101	50.3249	3.29
BOB1	2.6637	69.8734	16.6989	10.7640	1.26
BOB2	2.4031	86.7730	9.5915	1.2324	1.00
BOB3	4.1051	40.5098	28.6474	26.7377	3.74
BOB4	2.1640	86.0106	9.3989	2.4268	0.647

^{a} M: moisture; VM: volatile matter; FC: fixed carbon; TS: total sulphur.

this process, which also concentrates the carbon content. However, most OB comprises inorganic minerals with little to no organic carbon content, such as clays, sandstones, and shales. Because of this, fixed carbon was very low in overburden relative to coal.

The total sulfur of the samples varied from 0.64% to 6.94% (wt%). The coal samples exhibit relatively higher sulfur contents at an average of 4.62% than those of OB samples with an average of 1.6%. It is also observed that the subbituminous coal contains higher quantities of organic sulfur. The OB layers above coal seams are typically composed of sedimentary rocks like sandstones, shales, and clays deposited under various environmental conditions because of biochemical processes involving sulfur-reducing bacteria that incorporate sulfur into the plant material as it decomposes.[39,40] Unlike the coal-forming settings, these circumstances may not be as exposed to sulfur-bearing fluids or organic interactions in the OB layers. Because they lack substantial amounts of organic material and the environments necessary for the development of sulfur minerals, overburden materials often have lower sulfur contents.

XRD-mineralogy of coal and OB samples

In order to assess the mineral phases present in the coal and OB samples, representative samples (BOB1 and BOB2; BAC2 and BAC4) with higher total REY concentrations (Table 2) were analysed using powder-XRD (P-XRD). The results indicate that quartz (Q), haematite (He), pyrite (P), calcite (Ca), kaolinite (K), and magnetite (M) are the dominant mineral phases in each sample Fig. 2. A prominent, high-intensity peak at a 2θ value of approximately 26.6° in the XRD pattern confirms the presence
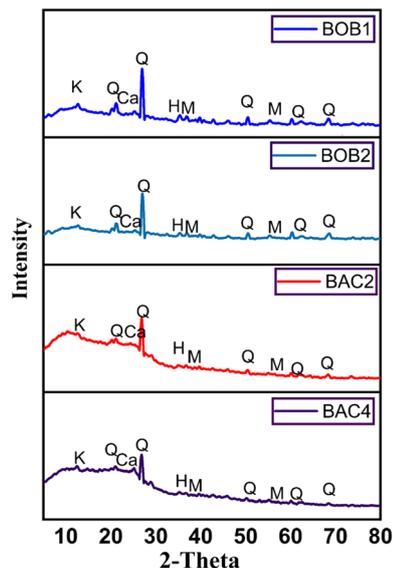

Fig. 2 Qualitative XRD-analysis of coal and OB samples showing the presence of mineral phases (Q: quartz; He: haematite; P: pyrite; Ca: calcite; K: kaolinite; M: magnetite).

of quartz, which was a major component in both coal and OB samples, exhibiting significant crystallinity. Additionally, the mineral phase intensity in coal samples is relatively lower than in OB samples Fig. 2, which was due to the coalification process, primarily occurring in low-oxygen environments such as swamps and peat bogs, where organic plant material accumulates and undergoes burial.[41] In contrast, OB refers to the layer of sedimentary rock (shale, sandstone, etc.) that lays above the

Table 2 Summary of the REY and trace elements concentrations (in mg kg⁻¹) of coal and overburden (OB) samples[a]

Sample ID	BOB1	BOB2	BOB3	BOB4	BAC1	BAC2	BAC3	BAC4	BAC5	Average	WCA*	CCA**	Maximum	Minimum
La	26.45	29.99	15.64	25.44	1.82	5.85	0.77	6.24	3.67	12.87	11	22.5	29.99	0.77
Ce	67.16	76.36	33.72	63.54	4.55	12.35	2.09	12.95	7.7	9	9	46.7	76.36	2.09
Pr	6.91	7.84	3.96	6.57	0.52	1.34	0.18	1.33	0.8	3.27	3.5	6.42	7.84	0.18
Nd	27.91	30.44	15.69	25.96	2.82	5.5	1.32	5.12	3.53	13.14	12	22.3	30.44	1.32
Sm	6.36	6.27	3.44	5.53	0.84	1.09	0.31	0.87	0.71	2.82	2	4.07	6.36	0.31
Eu	1.49	1.45	3.08	1.35	1.44	0.25	0.05	0.13	0.11	1.04	0.47	0.84	3.08	0.05
Gd	6.15	5.91	3.61	5.06	1.07	1.35	0.51	0.76	0.82	2.8	2.7	4.65	6.15	0.51
Tb	0.75	0.7	0.39	0.67	0.08	0.11	BDL	0.03	0.02	0.34	0.32	0.62	0.75	0.02
Dy	4.14	3.79	2.69	3.25	0.89	1.16	0.55	0.68	0.7	1.98	2.1	3.74	4.14	0.55
Ho	0.62	0.57	0.42	0.57	0.07	0.13	0.02	0.03	0.05	0.28	0.54	0.96	0.62	0.02
Er	1.59	1.53	1.2	1.36	0.34	0.53	0.21	0.28	0.31	0.81	0.93	1.79	1.59	0.21
Tm	0.12	0.1	0.06	0.17	BDL	BDL	BDL	BDL	BDL	0.11	0.31	0.64	0.17	0.06
Yb	1.12	1.04	0.99	0.96	0.21	0.35	0.15	0.19	0.24	0.58	1	2.08	1.12	0.15
Lu	0.06	0.05	0.03	0.15	BDL	BDL	BDL	BDL	BDL	0.07	0.2	0.38	0.15	0.03
Sc	19.46	15.91	13.19	15.26	4.17	5.35	3.74	3.07	3.26	9.27	—	—	19.46	3.07
Y	18.49	17.05	14.14	14.79	4.9	6.85	3.83	3.77	4.54	9.82	8.4	18.2	18.49	3.77
∑REY	188.77	198.99	112.26	170.63	23.71	42.21	13.71	35.46	26.44	90.24	68.5	135.89	198.99	13.71
Critical	54.37	54.96	37.19	47.38	10.47	14.4	5.96	10.01	9.21	NA	NA	NA	NA	NA
Uncritical	47.36	51.46	29.73	43.95	5.69	9.88	1.82	9.33	6.11	NA	NA	NA	NA	NA
Excessive	69.08	78.12	35.22	65.39	4.83	12.83	2.26	13.17	7.99	NA	NA	NA	NA	NA
Critical%	31.83	29.78	36.410	30.232	49.88	38.803	59.362	30.790	39.510	NA	NA	NA	NA	NA
Cout1	0.787	0.703	1.055	0.724	2.167	1.122	2.637	0.760	1.152	NA	NA	NA	NA	NA

[a] Where BDL is below the detectable limit of Agilent ICP-MS; SD is the standard deviation, WCA* is the world coal average, and CCA**: is the Chinese coal average.[45,48]

Table 3 Summary of the trace elements concentrations (in mg kg^{-1}) of coal and overburden (OB) samples

Sample ID	BOB1	BOB2	BOB3	BOB4	BAC1	BAC2	BAC3	BAC4	BAC5	Average	Maximum	Minimum	SD
Li	71.92	78.86	41.25	78.02	6.42	20.67	3.89	24.48	14.45	37.77	78.86	3.89	29.12
Be	2.26	1.72	1.13	1.23	0.35	0.93	0.69	0.29	0.69	1.03	2.26	0.29	0.6
Ti	418.35	424.21	396.31	458.92	112.8	300.88	55.13	281.55	215.33	295.94	458.92	55.13	135.95
Cr	225.58	262.04	124.72	222.78	11.2	102.09	0.8	29.85	39.84	113.21	262.04	0.8	95.69
Mn	1551.5	1250.2	395.98	273.52	54.48	37.13	41.54	38.31	22.67	407.27	1551.56	22.67	549.47
Co	67.17	54.37	16.4	17.69	2.25	3.21	1.48	3.57	1.51	18.63	67.17	1.48	23.47
Ni	377.4	289.8	67.88	98.81	21.56	56.95	9.68	18.92	24.76	107.31	377.4	9.68	125.58
Cu	62.35	61.45	26.17	39.6	12.78	10.65	8.61	11.33	11.3	27.14	62.35	8.61	20.81
Ga	20.5	20.6	11.56	20.09	1.13	4.64	0.58	4.33	3.13	9.62	20.6	0.58	8.17
Se	6.84	6.45	4.44	3.27	1.9	2.27	BDL	BDL	BDL	4.19	6.84	1.9	1.92
Sr	254.39	127.14	163.53	258.01	72.54	84.2	46.32	83.66	81.02	130.09	258.01	46.32	74.49
Zr	6.4	4.49	6.06	2.37	BDL	0.78	BDL	3.69	0.49	3.47	6.4	0.49	2.19
Cd	0.11	0.32	BDL	0.03	BDL	BDL	BDL	BDL	BDL	0.15	0.32	0.03	0.12
Tl	0.43	0.39	0.15	0.33	BDL	0.33	BDL	0.14	0.18	0.28	0.43	0.14	0.11
Pb	22.99	24.66	8.53	14.28	3.02	3.18	0.76	13.4	1.98	10.31	24.66	0.76	8.56
Bi	0.4	0.33	0.3	0.1	0.28	BDL	BDL	BDL	BDL	0.28	0.4	0.1	0.1
U	1.19	1.04	0.68	1.11	0.1	0.26	BDL	0.4	0.19	0.62	1.19	0.1	0.41

coal seam and it was generated from a different geological condition leading to the accumulation of minerals such as clay, silt, and sand[42] as a result OB typically contains multiple ranges of minerals from different sources over time. The composition of coal generally reflects the type of vegetation that contributed to its carbon-based organic matter. In contrast, coalmine OB consists of weathered minerals and rocks that do not undergo the same transformation process. As a result, the mineral content in OB is largely determined by the weathering of parent rocks.[43,44]

Insight into REY concentrations in coal OB and AMD water samples

The distribution of REY, along with heavy metals, in raw coal and overburden (OB) samples is detailed in Tables 2 and 3. Furthermore, the presence of REY and trace elements in adjacent AMD water samples is illustrated in Tables 4 and 5. The average REY concentration in AMD is 259.02 ppb (μg L^{-1}). Among these, the average light rare earth elements (LREY) concentration was 162.69 μg L^{-1} heavy rare earth elements (HREY) accounted for 24.77 μg L^{-1}. This indicates that the LREY concentration is approximately 5.7 times higher than that of HREY, highlighting a significant enrichment of lighter rare earth elements in the AMD water.

The REY concentration in coal and OB was found in the range between 13.71 mg kg^{-1} and 198.99 mg kg^{-1}, with an average value of 90.24 mg kg^{-1}. This variation indicates

differences in mineral composition and geochemical processes influencing REY distribution within the samples from the study area, this is significantly higher than the average of global (68.5 mg kg^{-1})[45] and USA coal (62.19 mg kg^{-1}).[45–47] If we compare separately, the average REY concentration in OB was 167.74 mg kg^{-1}, much higher than the REY of coal i.e. 28.30 mg kg^{-1}. Therefore, we can conclude that the OB of NER coalfield has huge potential sources of REY recovery as we can see that the concentration of REY in OB is 2.39 times higher than the global average concentration in coal.[45] In the meantime, REY can be further divided into critical (critical-Nd, Eu, Tb, Dy, Y and, Er), uncritical (uncritical-La, Pr, Sm, and Gd), and excessive (excessive-Ce, Ho, Tm, Yb, and Lu) conferring to the supply and demand. Coal-based materials with a proportion of critical REY greater than 30% and a prospect coefficient (C_{out1}) ratio of critical to excessive greater than 0.7 are considered to have the potential for REY. Table 2 shows that the concentration of REY in OB is higher than the world average concentration and the Chinese average concentration of REY in coal. Only the BOB3 sample from OB found less concentration compared with Chinese coal i.e. 112.26 mg kg^{-1}. Moreover, the concentration of critical REY (critical%) and prospect coefficient (C_{out1}, as shown in eqn (1)) in coal and coalmine OB, the critical% and C_{out1} were all above 30% and 0.7.

$$C_{out1} = \frac{critical}{excessive} \qquad (1)$$

Table 4 Summary of the REY concentrations in ppb (μg L^{-1}) of AMD water samples

Sample ID	La	Ce	Pr	Nd	Sm	Eu	Gd	Tb	Dy	Ho	Er	Tm	Yb	Lu	Sc	Y	$\sum$REY
MW1	128.8	197.24	22.72	79.44	14.18	3.7	17.89	2.68	14.94	2.82	7.22	0.86	5	0.71	27.41	123.67	649.26
KM1	19.22	40.55	4.18	17.39	4.21	1.19	5.79	0.83	4.36	0.78	1.82	0.2	1.09	0.14	1.67	31.49	134.91
SW1	23.31	49.23	5.32	23.24	6.84	2.08	10.16	1.64	9.26	1.69	4.1	0.47	2.75	0.37	23.71	74.31	238.48
AMD1	1.68	3.25	0.44	1.82	0.44	0.3	0.52	0.09	0.44	0.08	0.2	0.03	0.15	0.03	1.17	2.8	13.43
Average	43.25	72.56	8.16	30.48	6.42	1.82	8.59	1.31	7.25	1.34	3.33	0.39	2.25	0.31	13.49	58.07	259.02
Minimum	1.68	3.25	0.44	1.82	0.44	0.3	0.52	0.09	0.44	0.08	0.2	0.03	0.15	0.03	1.17	2.8	13.43
Maximum	128.8	197.24	22.72	79.44	14.18	3.7	17.89	2.68	14.94	2.82	7.22	0.86	5	0.71	27.41	123.67	649.26

Table 5 Summary of the trace elements concentrations in ppb ($\mu g\ L^{-1}$) of AMD water samples

Sample ID	Li	Be	B	Ti	Mn	Co	Ni	Cu	Zn	Ga	Se	Sr	Tl	U
MW1	200.7	7.59	8.9	2.07	51 199	964.81	5371.7	73.63	1556.84	4.69	4.39	1983.63	0.32	2.42
KM1	66.88	1.34	3.55	0.25	19 498.54	262.67	998.51	10.19	303.8	1.04	1.13	935	0.09	0.24
SW1	215.93	6.02	9.66	0	48 246.72	914.75	5340.31	73.49	1047.06	1.52	3.8	1791.75	0.26	1.54
AMD1	130.96	0.21	9.16	2.16	37 996.78	16.1	145.08	15.49	536.95	0.35	1.78	1694.08	0	0.22
Average	153.62	3.79	7.82	1.12	39 235.26	539.58	2963.9	43.2	861.17	1.9	2.77	1601.11	0.17	1.11
Minimum	66.88	0.21	3.55	0	19 498.54	16.1	145.08	10.19	303.8	0.35	1.13	935	0	0.22
Maximum	215.93	7.59	9.66	2.16	51 199	964.81	5371.7	73.63	1556.84	4.69	4.39	1983.63	0.32	2.42

where C_{out1} is the prospects coefficient, critical represents the total concentration of critical REY (Nd, Eu, Tb, Dy, Y, and Er), and excessive represents the total concentration of excessive REY (Ce, Ho, Tm, Yb, and Lu). Based on the market supply and demand relationship. Seredin and Dai proposed that a prospect coefficient (C_{out1}) greater than 0.7 has the potential for REY recovery.

To comprehensively assess the distribution of REY and heavy metals in coal and OB samples from the Makum coalfield, ICP-MS data were analysed to evaluate their variations in sample types. This analysis provides insights into the coal and OB deposits' geochemical characteristics and elemental distribution. The elements Tb, Tm, and Lu are present in OB (Table 2) however, the concentrations of these elements were found to be below the detectable limit (BDL) of the instrument in the coal sample (Table 3). Similarly, cadmium (Cd) and bismuth (Bi) were also reported to be BDL in the coal samples (Table 3). The heavy metal concentrations are considerably higher than previous findings from other coalfields in the NER.[1,12,49,50] The highest concentration of manganese (Mn) 1551.56 mg kg^{-1}, followed by Ti (458.92 mg kg^{-1}), Ni (377.40 mg kg^{-1}), Cr (262.04 mg kg^{-1}), Sr (258.01 mg kg^{-1}), Li (78.86 mg kg^{-1}), Cu (62.35 mg kg^{-1}), Zn (6.40 mg kg^{-1}), Co (67.17 mg kg^{-1}), Ga (20.60 mg kg^{-1}), Se (6.84 mg kg^{-1}), Be (2.26 mg kg^{-1}), Tl (0.43 mg kg^{-1}), U (1.19 mg kg^{-1}), and bismuth (Bi) (0.40 mg kg^{-1}), respectively, as shown in Table 3. The heavy metal in the study area was found higher concentrations in the OB sample compared to the coal sample. This is due to the genetic differences between the depositional environments of coal and OB. Coal is formed organically from plant materials, which have inherently low metal content, and the reducing conditions under coal dilute metal content and promote metal loss through leaching.[2,51,52] However higher metal concentration in OB results from its inorganic, mineral-rich composition of weathered igneous and metamorphic rocks as clastic and non-clastic sedimentation, which pay metal-bearing minerals that accumulated in the OB layer during the sediment deposition period.

REY geochemistry

The geochemical parameters of coal and OB samples are summarised in Table 6. The average value of LREE/HREE, LREE/MREE, and MREE/HREE are determined to be 31.80, 3.35, and 10.17 respectively, signifying characteristics of MREE–LREE enrichment and HREE depletion. The δEu values range from 0.03 to 3.55 (mean of 1.50) for the coal samples showing negative Eu anomalies, indicating that the study area was greatly affected by terrestrial materials. Also, the behaviour of the Eu in redox-sensitive environments can impact its distribution,[54] sometimes reducing circumstances can tend to the mobilization and removal of Eu, contributing to a negative anomaly. In contrast, the geochemical behaviour of Eu is influenced by redox conditions, as Eu can exist in both Eu^{2+} and Eu^{3+}, however Eu^{3+} is more stable in the oxidising geological system.[53,55] Europium (Eu^{2+}) easily substitutes calcium (Ca^{2+}) by replacement in Ca-rich rocks and sediments like marl, dolomite, limestone, and mafic rocks. The substitution is caused because mafic magmas come from reducing surroundings in the deep parts of the Earth. Because of this, Eu shows a positive anomaly to the neighbouring rare earth elements samarium (Sm) and gadolinium (Gd) due to sequestering into Ca^{2+} positions of Ca-rich feldspars. Contrariwise, Eu is defined by negative anomalies in highly oxygenated magmatic systems, *i.e.*, granites, aplites, tonalites-trondhjemites, and granodiorites (TTGs). They are high in alkali content but low in Ca content, which does not allow Eu incorporation. In sedimentary environments, Eu anomalies are directly inherited from their source areas of origin, as well as the geochemical signature of their provenance. Positive anomalies of Eu in OB samples indicate detrital input and reducing conditions in the depositional paleoenvironment favourable to the stabilization of Eu^{2+} (ref. 56) and it preferentially incorporated into minerals, leading to an enrichment of the Eu.[57]

Cerium (Ce) is generally found in two oxidation states: +3 (Ce^{3+}) and +4 (Ce^{4+}). Under oxic (oxygenated) conditions, Ce^{4+} is stable and readily precipitates out of solution. Under these conditions, seawater exhibits a negative Ce anomaly (Ce < 0) and sediments exhibit a positive Ce anomaly (Ce > 0), signifying an oxygenated water column. Under anoxic (oxygen-poor) conditions, Ce^{3+} is more stable and dissolved in seawater. As a result, seawater exhibits a positive Ce anomaly, and sediments also exhibit a positive anomaly due to the lack of Ce precipitation from seawater, signifying an anoxic water column. Nevertheless, numerous factors might influence these global patterns, such as secondary oxidation, weathering, diagenetic processes, ocean column depth, and geologic age. These processes are capable of modifying Ce anomalies in shales, coals, and other marine sediments and result in variations from the predicted pattern. The mean value of δCe ranges between 0.57 to 26.34 (mean of 5.29), where most of the OB samples were negatively enriched. This led to the preferential removal of Ce relative to other REY in an organic-rich environment in the presence of

Table 6 Summary of geochemical parameter of REY in coal and OB samples from Makum coalfield, NER[a]

Sample ID	$\sum$LREE	$\sum$MREE	$\sum$HREE	L/M	L/H	M/H	Ce/La	Y/Ho	(La/Lu)$_u$
BOB1	134.79	31.02	3.51	4.35	38.40	8.84	2.54	29.82	4.41
BOB2	150.90	28.90	3.29	5.22	45.87	8.78	2.55	29.91	6.00
BOB3	72.45	23.91	2.70	3.03	26.83	8.86	2.16	33.67	5.21
BOB4	127.04	25.12	3.21	5.06	39.58	7.83	2.50	25.95	1.70
BAC1	10.55	8.38	0.62	1.26	17.02	13.52	2.50	70.00	nd
BAC2	26.13	9.72	1.01	2.69	25.87	9.62	2.11	52.69	nd
BAC3	4.67	4.94	0.38	0.95	12.29	13.00	2.71	191.50	nd
BAC4	26.51	5.37	0.50	4.94	53.02	10.74	2.08	125.70	nd
BAC5	16.41	6.19	0.60	2.65	27.35	10.32	2.10	90.80	nd
Average	63.27	15.95	1.76	3.35	31.80	10.17	2.36	72.22	4.33
Maximum	150.90	31.02	3.51	5.22	53.02	13.52	2.71	191.50	6.00
Minimum	4.67	4.94	0.38	0.95	12.29	7.83	2.08	25.95	1.70

Sample ID	(La/Sm)	(Gd/Lu)$_u$	(Gd/Yb)$_u$	ET	δEu	δCe	δGd	(La/Yb)$_c$	δCe/δEu
BOB1	0.63	7.94	2.69	M	3.36	0.64	7.02	16.34	0.19
BOB2	0.73	9.16	2.78	M	3.22	0.57	6.64	19.95	0.18
BOB3	0.69	9.33	1.79	M	3.55	0.95	2.37	10.93	0.27
BOB4	0.70	2.61	2.58	M	2.69	0.66	5.15	18.34	0.25
BAC1	0.33	nd	2.50	M	0.42	8.40	0.22	6.00	19.91
BAC2	0.81	nd	1.89	M	0.14	2.75	0.34	11.57	19.89
BAC3	0.38	nd	1.67	M	0.00	26.34	0.03	3.55	586.3
BAC4	1.09	nd	1.96	M	0.05	2.73	0.14	22.73	54.45
BAC5	0.78	nd	1.67	M	0.03	4.58	0.11	10.58	133.84
Average	0.68	7.26	2.17	—	1.50	5.29	2.45	13.33	90.59
Maximum	1.09	9.33	2.78	—	3.55	26.34	7.02	22.73	586.37
Minimum	0.33	2.61	1.67	—	0.05	0.57	0.03	3.55	0.18

[a] $\sum$REY is the total content of $\sum$REY = La + Ce + Pr + Nd + Sm + Eu + Gd + Tb + Dy + Y + Ho + Er + Tm + Yb + Lu + Sc (mg kg^{-1}); $\sum$LREE = La + Ce + Pr + Nd + Sm; $\sum$MREE = Eu + Gd + Tb + Dy + Y; $\sum$HREE = Ho + Er + Tm + Yb + Lu; L/H = LREE/HREE; L/M = LREE/MREE; M/H = MREE/HREE; δEu is anomaly of Eu element which is δEu = Eu/Eu* = Eu$_u$/(0.67 × Sm$_u$ + 0.33 × Tb$_u$); δCe is anomaly of Ce element which is δCe = Ce/Ce* = Ce$_u$/(La$_u$ × Pr$_u$)$^{1/2}$; L = light REY enrichment; M = medium REY enrichment type. Subscript u values are normalized by the UCC content of REY whereas c values are normalized by the average REY concentration of chondrite.[48,53]

organic matter which can form a reducing environment in paleoenvironmental conditions. It can specify fluctuations in redox conditions and organic matter content, which influence the mobility and distribution of REYs. Under reducing environments, Ce tends to stay in the more soluble Ce^{3+} form, which can be favoured for weathering conditions of the system.[58] This implies that the OB formed in an environment sub-oxic to mildly anoxic conditions, such as swamps or peat bogs in the Makum coalfield, the negative anomalies may suggest the preferential leaching of cerium into minerals or the water systems, or an interplay of these during diagenesis while other REY remains in the environment leading to its relative depletion in the coalmine OB.[8,57,59–61] Positive Ce (δCe) anomalies in coal samples can imply the oxidizing conditions during deposition.[62] Under oxic conditions, Ce can be oxidized to Ce^{4+}, which is less soluble and can precipitate from the solution, enriching it in the solid phase.[63,64]

Paleo redox conditions

REY is often used to indicate the sedimentary setting and accumulation process. Owing to their unchanging chemical properties, they are easily disturbed by different geological processes. Among the REY, Ce, and Eu are more sensitive to change in the

redox environment and are frequently used in studies of the paleoenvironment sedimentary deposits of coal seam.[65–68]

To know the depositional environment, we have studied the ratio of δCe to δEu (δCe/δEu), which ranges from 586.37 to 19.8 for the coal, and 0.26 to 0.17 for the OB samples. The correlation between δCe/δEu and $\sum$REY is shown in Fig. 3 and the point at which the coal sample is greater than 1, indicates that the environment during the coal depositional period was inclined to reduction[47,69] and the coal deposition environment was more reducing than the OB formation. When Ce/La < 1.5, it represents an oxygen-rich environment, when 1.5 < Ce/La < 2, it represents an anaerobic environment; and when Ce/La > 2, it means an anaerobic environment.[70] The Ce/La ratios in the study area range from 2.07 to 2.71 (average of 2.3). Thus, in Fig. 4, all the points lie in the reducing environment. This study also confirmed that a reducing environment existed during the coal and OB depositional period, which probably had an impact on REY geochemical behaviour and mineralogical makeup.

Distribution pattern of REY

The historical supply of REY and the evolution in the sedimentary environment can be reflected in their distribution[71] As shown in Fig. 5 and 6, which are the Upper Continental Crust
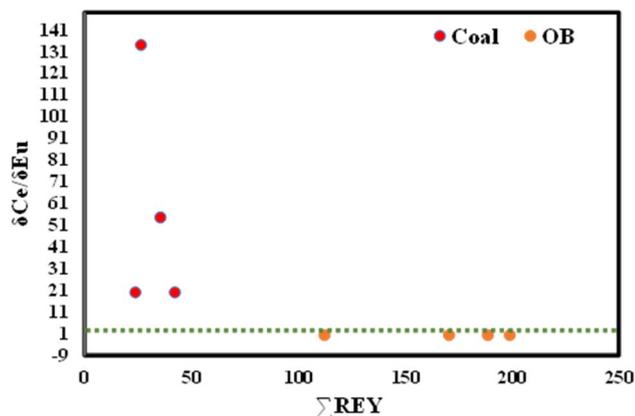
Fig. 3 Correlation between $\delta Ce/\delta Eu$ and $\sum REY$ (modified after Mu *et al.*,[48] indicates that the environment during the coal depositional period was inclined to reduction).

(UCC) and chondrite normalization of REY, these normalization in coal and OB show similar trends under both normalizations. In particular, the coal and OB samples both reflect a relative overabundance of middle rare earth elements (MREY)

and underabundance of heavy rare earth elements (HREY). The REY distributions, normalized to one another, are characterized by a distinct zigzag pattern mainly dominated by M-type enrichment. This is inferred from the typical inverted V-shaped anomaly in the peaks of normalization between Sm and Tb in all the samples studied. In addition, a comparative evaluation of UCC and chondrite-normalized data validates that coal samples exhibit lower levels of REY enrichment compared to OB samples, thus suggesting differential geochemical behaviours among the two different sample matrixes.

Yttrium (Y) is connected with lanthanides in the environment as the ionic radius is very similar and the ionic charge is equal to that of Ho, for this reason, Y is usually placed between Dy and Ho.[74] A three-fold geochemical classification of REY was used in this study that includes light (L-REY: La, Ce, Pr, Nd, and Sm), medium (M-REY: Eu, Gd, Tb, Dy, and Y), and heavy (H-REY: Ho, Er, Tm, Yb, and Lu) REY enrichment[53] where, three enrichment types including L-type $((La/Lu)_n > 1)$, M-type $((La/Sm)_n < 1$ and $(Gd/Lu)_n > 1)$, and H-type $((La/Lu)_n < 1)$ are considered in comparison with UCC.[53] According to this three-fold classification proposed by ref. 48 and 53 we have reported that the coal and OB samples of the current study area
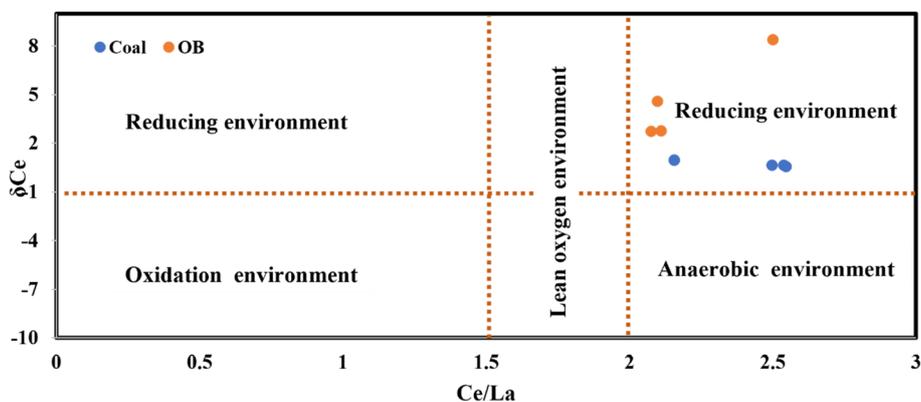
Fig. 4 Scatter distribution of Ce/La and δCe (modified after Mu *et al.*[48] indicate that all the coal and coalmine OB samples lie in the reducing environment).
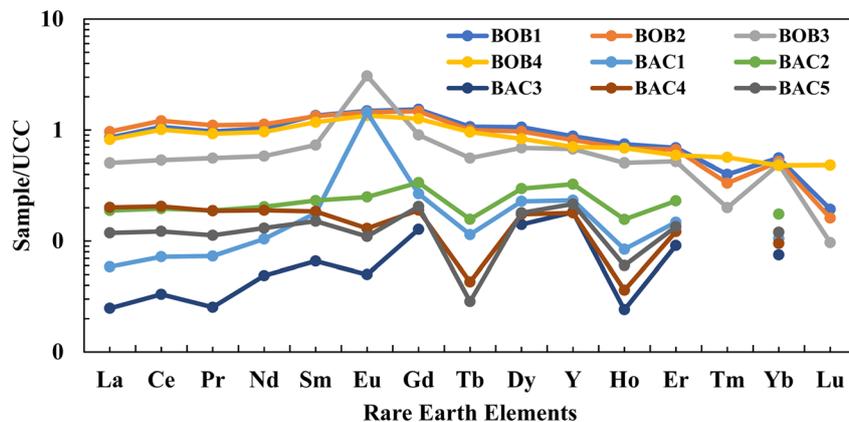
Fig. 5 UCC normalized REY distribution plot for raw coal and OB samples showing higher enrichment of OB (BOB1, BOB2, BOB3, and BOB4) sample compared to coal (BAC1, BAC2, BAC3, BAC4, and BAC5) samples. UCC normalisation values are taken from Taylor and McLennan (1985).[72]
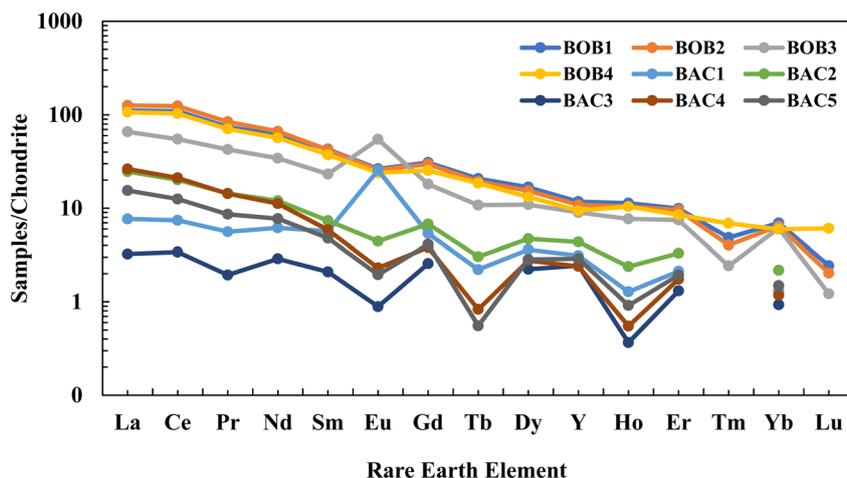
Fig. 6 Chondrite normalized REY distribution plot for raw coal and OB samples showing higher enrichment of OB (BOB1, BOB2, BOB3, and BOB4) sample compared to Coal (BAC1, BAC2, BAC3, BAC4, and BAC5) samples (chondrite normalization values after Anders and Grevesse, 1989).[73]

show middle-type (M-REY) enrichment with REY (Table 6). This is supported by a broad, sharp, inverted V-shape and regular V-shape curve as shown in Fig. 5 of UCC normalisation and Fig. 6 of chondrite normalisation of coal and OB samples. The Sm to Dy portions of the curves were steep and smooth, respectively, showing that the fractionation of MREY was high and that of HREY. The differences in REY concentrations in the samples suggest that the lower parts (coal seam) have relatively lower REY concentrations than the upper parts (OB layers), implying some fractionation of REY. In addition, in samples BOB1 to BOB4, which are carbonaceous mudstone, the greater REY concentration in OB samples compared to coal implies that lithological and environmental variations also significantly contribute to REY distribution.[75]

Although the fractionation trends are similar, the chondrite normalized distribution pattern of coal and OB samples show very distinct REY distribution patterns for Eu anomalies. Using Eu anomalies, the samples can be classified into three

categories such as Eu-slight negative (BOB1, BOB2, and BOB4) Eu-negative (BAC2, BAC3, BAC4, and BAC5), and Eu positive (BAC1, and BOB3) high magnitude anomalies as shown in Fig. 5 and 6. Negative Eu anomaly indicates the fractionation/absence of plagioclase and amphibole in the sediment being transported or a felsic to intermediate provenance, which is responsible for the supply of sediments. Contrary to this, the positive Eu-anomaly indicates the inclusion of plagioclase in the sediment or the presence of mafic source rocks in the provenance that supplied the sediment. In the present case, the provenance for the OB is an intermediate source, and the mineral matter in the coal samples is derived from a felsic and mafic provenance or a mixed provenance. The change in provenance in the case of coal samples (mineral matter) is well depicted through both their Eu positive and negative signatures on the REY distribution in the normalization plot diagram above.

Table 7 Pearson correlation matrix between the different geochemical parameters of REY of coal and OB samples

	$\sum$REY	$\sum$LREE	$\sum$MREE	$\sum$HREE	L/M	L/H	M/H	Ce/La	Y/Ho	$(La/Sm)_u$	$(Gd/Yb)_u$	δEu	δCe	δGd	$(La/Yb)_c$	δCe/δEu
$\sum$REY	1.0															
$\sum$LREE	1.0	1.0														
$\sum$MREE	1.0	1.0	1.0													
$\sum$HREE	1.0	1.0	1.0	1.0												
L/M	0.7	0.8	0.6	0.7	1.0											
L/H	0.6	0.6	0.4	0.5	1.0	1.0										
M/H	−0.8	−0.8	−0.8	−0.8	−0.8	−0.6	1.0									
Ce/La	0.3	0.3	0.3	0.3	−0.1	−0.2	0.2	1.0								
Y/Ho	−0.7	−0.7	−0.8	−0.8	−0.5	−0.4	0.7	0.1	1.0							
$(La/Sm)_u$	0.1	0.1	0.0	0.0	0.7	0.8	−0.5	−0.7	−0.2	1.0						
$(Gd/Yb)_u$	0.8	0.8	0.7	0.7	0.5	0.4	−0.3	0.5	−0.6	−0.2	1.0					
δEu	0.9	0.9	1.0	1.0	0.6	0.4	−0.7	0.3	−0.7	0.0	0.6	1.0				
δCe	−0.6	−0.6	−0.6	−0.6	−0.7	−0.7	0.8	0.5	0.9	−0.6	−0.4	−0.5	1.0			
δGd	1.0	1.0	1.0	1.0	0.7	0.5	−0.7	0.4	−0.7	0.0	0.8	0.9	−0.5	1.0		
$(La/Yb)_c$	0.6	0.6	0.5	0.5	1.0	1.0	−0.7	−0.2	−0.4	0.8	0.5	0.4	−0.7	0.5	1.0	
δCe/δEu	−0.5	−0.5	−0.5	−0.5	−0.6	−0.6	0.6	0.4	0.9	−0.4	−0.5	−0.5	1.0	−0.4	−0.6	1.0

Pearson correlation of REYs in coal and OB samples

Elemental geochemical ratios play a significant role in understanding their incorporation into the geological system, and geo-environmental conditions in which these REY are hosted by minerals because elements such as REY do not form minerals on their own but they will be accommodated in crystal lattices of other minerals or they can form minerals in a combination of other elements. Light REE and heavy REE behave differently in different geochemical conditions and their sequestration into various minerals differently whether it's magma genesis or low-temperature geological processes like hydrothermal or sedimentary environments. Using the geochemical data sets through Pearson correlation (PC) analysis. Typically, the PC ranges from −1 to +1, where +1 indicates a very strong positive linear relationship, while −1 denotes a strong negative linear relationship. A PC value of zero indicates no correlation, reflecting a random distribution of data points.[76] The correlation analysis performed on the sample data were revealed elaborately in Table 7. In particular, the correlation that has been noted between $\delta Ce/\delta Eu$ and $\sum REY$ is reported as −0.5, revealing that there exists a moderate negative correlation between these two specific variables. This relationship can perhaps be attributed to differences that take place in oxidation states, changes in the pH levels, or other predominant environmental conditions that may differentially affect the geochemical properties of both Ce and Eu.[69,77]

The three REE groups LREEs (La to Eu), MREEs (Gd to Ho), and HREEs (Er to Lu) behave differently in differing geological environments such as soil rock and water also in rocks variedly in igneous rocks, sediments, and metamorphic rocks. In this study, a good positive correlation between LREE, MREE, and HREE and their ratios indicate their genesis in a similar geological environment or the source is the same. The parameters studied such as Europium and Cerium anomalies are the best proxies for oxidative/reductive conditions and seawater composition being operated during the deposition of sediments.

It also indicates the influence of redox circumstances, fractionation, and fluid–mineral interactions on the circulation of REYs[61,77] Cerium anomalies (δCe) and $\sum REY$ shows a negative correlation (−0.6) implying the overall concentration of REY inclines to decrease. This suggests that geochemical processes driving δCe, such as oxidation and precipitation can also contribute to the removal of REY from the depositional environment in the Makum coalfield.[78]

Observations on REY chemistry using FESEM, HR-TEM, and XPS analysis

This work is interesting since it is the first to use FE-SEM and XPS techniques on coal and OB samples to identify the REY in the study area. This technique offers hitherto unknown insights into REY's chemical and microstructural states, which are essential for evaluating their potential for extraction and environmental effects. These techniques enable the investigation of REY at the microstructural and surface level chemistry, providing a new perspective on their morphology and chemical state, which cannot be achieved using traditional bulk analysis
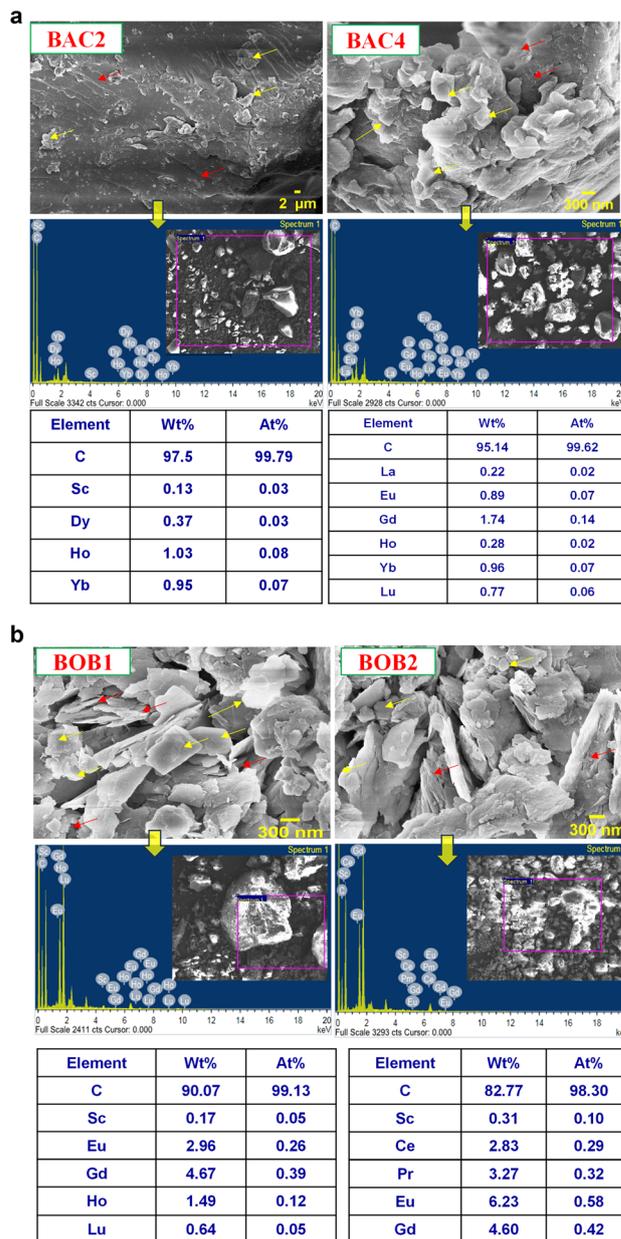
Fig. 7 (a) FE-SEM images of coal (BAC2 and BAC4) samples along with the EDS analysis with an elemental concentration of some REY. (b) FE-SEM images of OB (BOB1 and BOB2) samples along with the EDS analysis with the elemental concentration of some REY.

methods. Combining FE-SEM images with XPS's surface-sensitive chemical analysis integrates microstructural and chemical data, creating a comprehensive understanding of REY behaviour in coal and OB.

Based on the maximum REY concentration values obtained by ICP-MS analysis (see Table 2), two representative coal and overburden (OB) samples were selected for further characterization by FE-SEM and XPS techniques. The respective FE-SEM micrographs, accompanied by EDS analysis, are shown in Fig. 7(a) and (b) for coal and OB samples. These micrographs show a variety of microstructural morphologies, evidencing the
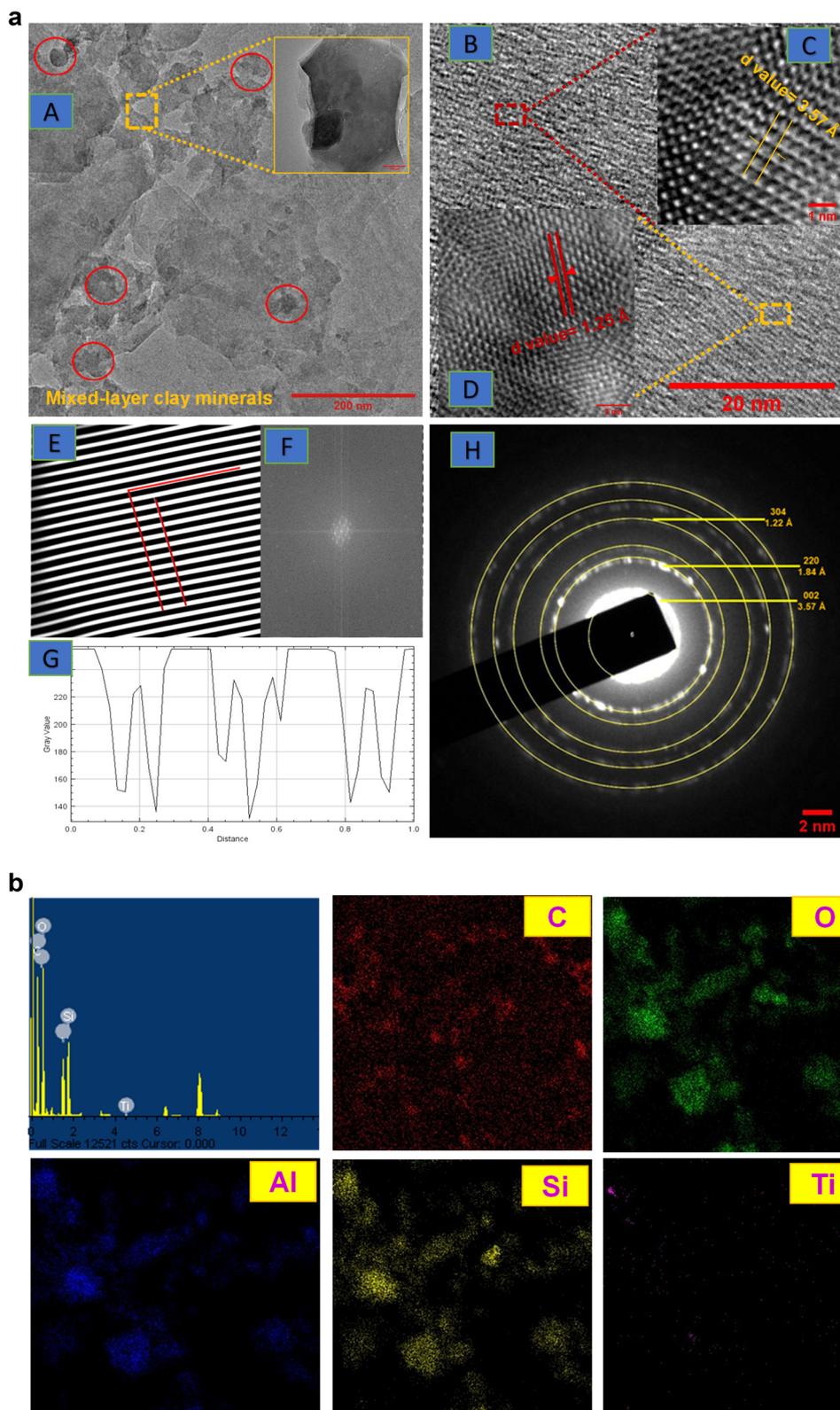
Fig. 8 (a) HR-TEM image showing the presence of mixed-layer minerals at 200 nm (A). (B) High-resolution image at 20 nm, revealing disordered crystal fringes. Insets (C) and (D) display d-spacing values of 3.57 Å and 1.25 Å, respectively. (E), (F), and (G) show the reverse FFT, FFT, and gray value scale for d-spacing calculation. (H) The selected area electron diffraction (SAED) pattern confirms the polycrystalline nature of the sample. (b) Transmission Electron Microscopy-Energy Dispersive X-ray Spectroscopy (TEM-EDS) investigation and elemental mapping of carbon (C), oxygen (O), aluminum (Al), silicon (Si), and titanium (Ti).

occurrence of nano-minerals and ultrafine units in the matrices of coal and OB. Aluminosilicate type minerals including kaolinite, orthoclase, and plagioclase were found, showing their rich occurrences in the samples.[14] Other minerals containing sulfate minerals, like rozenite [$FeSO_4 \cdot 4H_2O$], hematite [Fe_2O_3], pyrite [FeS_2], gypsum [$CaSO_4 \cdot 2H_2O$], and melanterite [$FeSO_4 \cdot 7H_2O$], are also present in both coal and OB samples supported by XRD analysis of Makum coalfield of Northeast India.[1,3,10,12,49,79]

A closer look at the individual EDS spectrum (Fig. 7(a) and (b)) confirms the presence of REYs, including La, Ce, Nd, Pr, Gd, Dy, Ho, Sc, Lu, Eu, and Yb, signifying that samples contain REY-bearing minerals in low quantity. In the above Fig. 7(a) and (b) quartz (yellow arrow) three-dimensional bright structure and kaolinite (red arrow) were predominantly observed in stratified and flaky conglomerates layered phyllosilicate clay-type Platy, book-like, or flaky aggregates due to its layered structure minerals are identified within 300 nm.

High-resolution transmission electron microscopy (HR-TEM) is used to study the crystallinity of the sample. The HR-TEM images revealed the irregular disorder shapes of multiple clay mineral particles probably kaolinite ($Al_2Si_2O_5(OH)_4$), quartz (SiO_2), *etc.* as mentioned earlier in XRD analysis Fig. 1. Fig. 8(a) showing the HR-TEM image at different nano-meter (nm) size confirms the presence of some nanoparticle including minerals. The HR-TEM image shows the presence of mixed-layer minerals at 200 nm (A) with different surface morphologies shown in red circular rings with disordered crystal fringes seen at 20 nm high-resolution image (B).

Insets (C) and (D) demonstrated *d*-spacing values of 3.57 Å (002, planes) possibilities for kaolinite ($Al_2Si_2O_5(OH)_4$) minerals and 1.25 Å (304 planes) for quartz (SiO_2), respectively. (E), (F), and (G) show the reverse FFT, FFT which shows multiple crystalline lattice dots confirming the polycrystalline nature of the sample, and gray value scale for *d*-spacing value calculation. (H) Selected Area Electron Diffraction (SAED) pattern forms concentric rings consisting of multiple crystallites oriented randomly confirming the polycrystalline nature of the sample it also shows another plane 220 at a *d*-spacing value is 1.82 shows the characteristics of rutile (TiO_2).

To understand the elemental configuration and corresponding elemental maps that illustrate the spatial distribution of these elements within the sample, we studied the TEM-EDS spectrum. The EDS confirms the presence of C, O, Al, Si, and Ti. The presence of Al and Si suggests that occurrences of aluminosilicate minerals, likely feldspar or clay minerals like kaolinite ($Al_2Si_2O_5(OH)_4$), and quartz (SiO_2). Ti-rich regions indicate the presence of titanium-bearing minerals like rutile (TiO_2), these elements show a strong association with REY. The O distribution aligns with the expected chemical bonding with other minerals as oxides, while the C distribution is generated from either an organic component or carbonate minerals. The elemental distribution seen provides some indication of the mineralogical and geological evolution of the sample. The Al and Si co-occurrence indicates a primary silicate matrix, and the development of the Ti enrichment in certain zones may
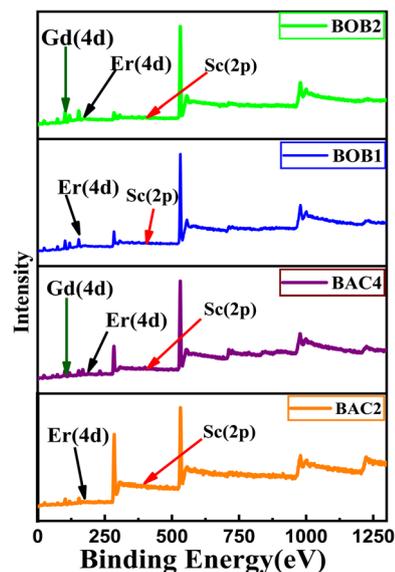
Fig. 9 The XPS survey spectra of the coal [BAC2 (Er_{4d}, Sc_{2p}), BAC4 (Er_{4d}, Sc_{2p}, Gd_{4d})] and OB [BOB1(Er_{4d}, Sc_{2p}), BOB2 (Er_{4d}, Sc_{2p}, Gd_{4d})] samples indicating the presence of Er (4d), Gd (4d), and Sc (2p).

represent either primary magmatic differentiation or secondary alteration processes.

Additionally, the nature of chemical bondings of REY in coal and OB samples was determined using XPS. Four representative samples of coal and OB selected based on higher $\sum REY$ concentrations were reported in ICPMS analysis (see Table 2) for further XPS analysis. The XPS survey spectra of the sample indicate the presence of $Er_{(4d)}$, $Gd_{(4d)}$, and $Sc_{(2p)}$ Fig. 9 in the coal and the OB samples.

On the other hand, the high-resolution deconvolution spectra of $Er_{(4d)}$ spectra split into three main peaks located at 168 eV for Er, 168.6 eV for Er_2O_3, and 170 eV corresponding for Er metal, respectively,[80,81] for both coal samples shown in Fig. 10(a) and for OB samples in Fig. 10(b). Similarly, XPS deconvoluted spectra of the $Sc_{(2p)}$ peak at 399 eV corresponding to (Sc), 400 eV to (ScN), and 402 eV to (Sc_2O_3), respectively. For the $Gd_{(4d)}$ spectra, it also split into two peaks at 140 eV corresponding to Gd metal and 141.5 eV to Gd_2O_3.[81]

Thus, XPS analysis corresponds with the ICPMS data for coal and OB samples. The two samples (BOB2 and BAC4) confirmed the presence of $Gd_{(4d)}$ as oxides. Er is detected *via* Er $3d_{5/2}$ and Er $3d_{3/2}$ peaks typically appear around 169 eV with an Er^{3+} oxidation state confirming presence of Er_2O_3, which support the study area is geochemically enriched with REY. Similarly, Sc and Gd, also show the presence of Sc^{3+} and Gd^{3+} as +3 oxidation states confirmatory to presence of Sc_2O_3 (binding energy at 402 eV) and Gd_2O_3 (binding energy at 140 eV). In addition, at 400 eV, we have seen another deconvoluted peak of Sc with oxidation +3 confirming presence of ScN. Based on the data obtained from XPS observation, it can be concluded that the REY present in the samples from NER region predominantly exhibits a +3 oxidation state and spectral data reveal that these elements formed
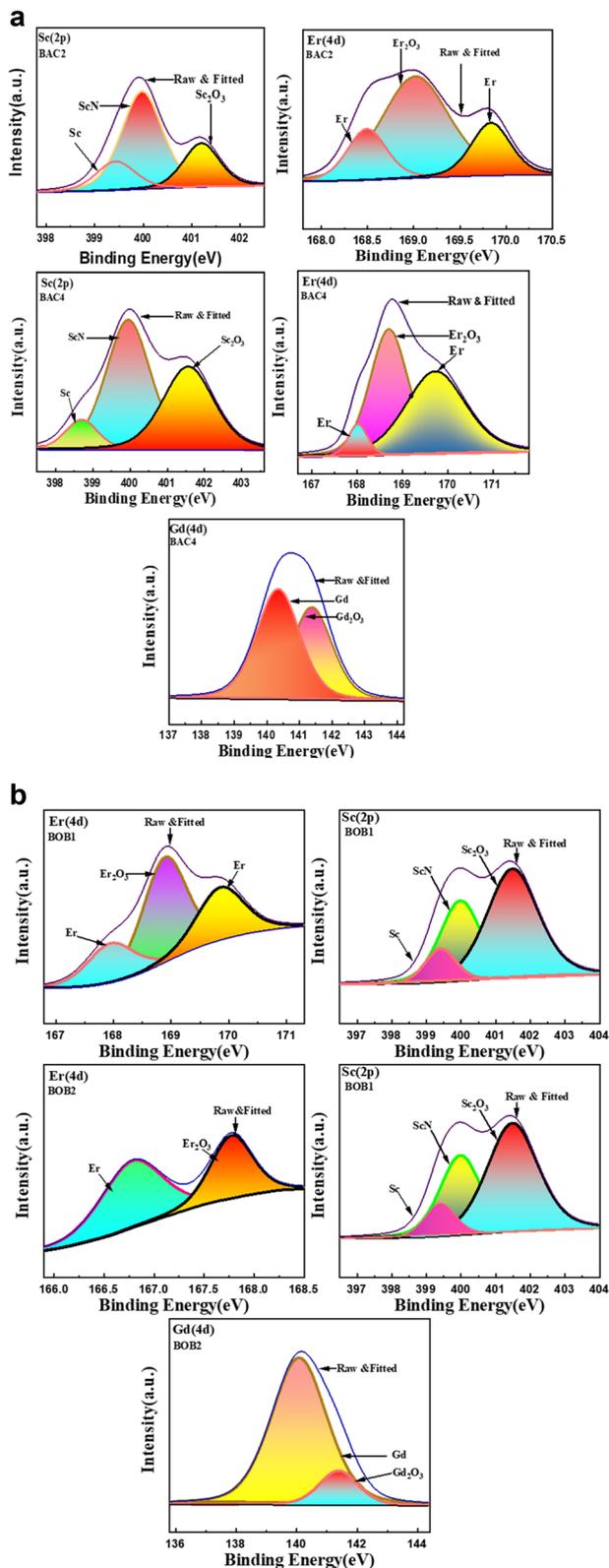
Fig. 10 (a) The XPS deconvoluted spectra of the coal (BAC2, and BAC4) samples show the presence of Sc_{2p}, Er_{4d}, and Gd_{4d}. (b) The XPS deconvoluted spectra of the OB (BOB1, BOB2) samples show the presence of Sc_{2p}, Er_{4d}, and Gd_{4d} at different types of bonding.

chemical bonds with oxygen, resulting in the compound REY_3O_4.

Conclusions

The occurrence and distribution of critical and rare earth elements in coal and overburden (OB) samples from the Makum coalfield in Northeast India are presented to assess their potential and geochemical behaviors. The average concentration of rare earth elements (REY) is 167.6 mg kg^{-1} in the OB samples and 28.31 mg kg^{-1} in the raw coal samples. Notably, the OB samples are more enriched in REY than the coal. In addition to REY, other critical elements like lithium show potential economic value, with an average concentration of 67.51 mg kg^{-1} in OB samples compared to 13.9 mg kg^{-1} in coal. The correlation between $\delta Ce/\delta Eu$ and REY suggests that the depositional environment of coal is more reducing in nature than that of the OB. Moreover, the formation of the coal seam is primarily characterized by M-type REE enrichment, followed by H-type. Therefore, a detailed and comprehensive study of various geochemical parameters of REY in OB is necessary to facilitate their recovery.

The results indicate that coal and overburden (OB) have the potential to serve as alternative repositories for rare earth elements and yttrium (REY), complementing the growing knowledge of REY occurrences in unconventional sources. Additionally, this study creates opportunities for sustainable resource recovery plans, especially in regions with substantial coal reserves. To fully unlock the economic potential of REY, future research should focus on broadening the dataset across different geological settings and exploring cost-effective extraction techniques.

Data availability

The data supporting this article, including elemental data generated through ICPMS, are available within the manuscript. The Upper Continental Crust (UCC) composition data are available at **https://doi.org/10.1017/S0016756800032167**.

Conflicts of interest

There are no conflicts to declare.

Acknowledgements

References

1 N. Bhuyan, N. Islam, M. Saikia, J. C. Hower and B. K. Saikia, Geochemical and mineralogical evaluations of coal, shale, and mine waste overburden from Makum coalfield of the Northeast India, *Int. J. Coal Sci. Technol.*, 2023, **10**(1), 44, DOI: 10.1007/s40789-023-00602-8.

2 S. Dai, J. C. Hower, R. B. Finkelman, *et al.*, Organic associations of non-mineral elements in coal: A review, *Int. J. Coal Geol.*, 2020, **218**, 103347, DOI: 10.1016/J.COAL.2019.103347.

3 B. K. Saikia, P. Wang, A. Saikia, *et al.*, Mineralogical and elemental analysis of some high-sulfur Indian Paleogene coals: A statistical approach, *Energy Fuels*, 2015, **29**(3), 1407–1420, DOI: 10.1021/EF502511T/ASSET/IMAGES/LARGE/EF-2014-02511T_0006.JPEG.

4 B. K. Saikia, A. Saikia, R. Choudhury, *et al.*, Elemental geochemistry and mineralogy of coals and associated coal mine overburden from Makum coalfield (Northeast India), *Environ. Earth Sci.*, 2016, **75**(8), 1–21, DOI: 10.1007/S12665-016-5484-X/METRICS.

5 U. S. Geological Survey, *Mineral Commodity Summaries 2021*, 2021.

6 Ministry of Coal, Government of India, accessed November 28, 2024, https://coal.gov.in/en/major-statistics/coal-reserves.

7 Ministry of Coal, *391 Coal Mines Operational in Northeast Region*, 2022, https://coal.gov.in/sites/default/files/2022-04/PIB1813250.pdf#page=1.00.

8 D. Bai, T. Wang, C. Li and W. Wang, Impact of coal energy development on the surrounding environmental water resources carrying capacity, *Desalin. Water Treat.*, 2024, **319**, 100518, DOI: 10.1016/J.DWT.2024.100518.

9 S. Goswami, Impact of Coal Mining on Environment, *European Researcher*, 2015, **92**(3), 185–196, DOI: 10.13187/ER.2015.92.185.

10 M. Dutta, J. Saikia, S. R. Taffarel, *et al.*, Environmental assessment and nano-mineralogical characterization of coal, overburden and sediment from Indian coal mining acid drainage, *Geosci. Front.*, 2017, **8**(6), 1285–1297, DOI: 10.1016/J.GSF.2016.11.014.

11 M. Dutta, N. Islam, S. Rabha, *et al.*, Acid mine drainage in an Indian high-sulfur coal mining area: Cytotoxicity assay and remediation study, *J. Hazard. Mater.*, 2020, **389**, 121851, DOI: 10.1016/J.JHAZMAT.2019.121851.

12 N. Islam, S. Rabha, K. S. V. Subramanyam and B. K. Saikia, Geochemistry and mineralogy of coal mine overburden (waste): A study towards their environmental implications, *Chemosphere*, 2021, **274**, 129736, DOI: 10.1016/J.CHEMOSPHERE.2021.129736.

13 B. K. Saikia, C. R. Ward, M. L. S. Oliveira, *et al.*, Geochemistry and nano-mineralogy of feed coals, mine overburden, and coal-derived fly ashes from Assam (North-east India):

14 A. Mahanta, D. Sarmah, N. Bhuyan, *et al.*, Geochemical and petrological studies of high sulfur coal and overburden from Makum coalfield (Northeast India) towards understanding and mitigation of acid mine drainage, *Int. J. Coal Sci. Technol.*, 2024, **11**(1), 1–15, DOI: 10.1007/S40789-023-00658-6/FIGURES/6.

15 F. Wall, Rare Earth Elements, *Encyclopedia of Geology*, 2nd edn, 2021, vol. 1–6, pp. 680–693, DOI: 10.1016/B978-0-08-102908-4.00101-6.

16 V. Balaram, Rare earth elements: A review of applications, occurrence, exploration, analysis, recycling, and environmental impact, *Geosci. Front.*, 2019, **10**(4), 1285–1303, DOI: 10.1016/j.gsf.2018.12.005.

17 B. Fu, J. C. Hower, W. Zhang, G. Luo, H. Hu and H. Yao, A review of rare earth elements and yttrium in coal ash: Content, modes of occurrences, combustion behavior, and extraction methods, *Prog. Energy Combust. Sci.*, 2022, **88**, 100954, DOI: 10.1016/J.PECS.2021.100954.

18 Y. Tao, L. Shen, C. Feng, *et al.*, Distribution of rare earth elements (REEs) and their roles in plant growth: A review, *Environ. Pollut.*, 2022, **298**, 118540, DOI: 10.1016/J.ENVPOL.2021.118540.

19 S. E. Humphris, The Mobility of the Rare Earth Elements in the Crust, *Rare Earth Element Geochemistry*, 1984, vol. 2, pp. 317–342, DOI: 10.1016/B978-0-444-42148-7.50014-9.

20 Y. Kanazawa and M. Kamitani, Rare earth minerals and resources in the world, *J. Alloys Compd.*, 2006, **408–412**, 1339–1343, DOI: 10.1016/J.JALLCOM.2005.04.033.

21 A. R. Chakhmouradian and F. Wall, Rare Earth Elements: Minerals, Mines, Magnets (and More), *Elements*, 2012, **8**(5), 333–340, DOI: 10.2113/GSELEMENTS.8.5.333.

22 L. Zheng, G. Liu, C. L. Chou, C. Qi and Y. Zhang, Geochemistry of rare earth elements in Permian coals from the Huaibei Coalfield, China, *J. Asian Earth Sci.*, 2007, **31**(2), 167–176, DOI: 10.1016/J.JSEAES.2007.06.001.

23 K. M. Goodenough, F. Wall and D. Merriman, The Rare Earth Elements: Demand, Global Resources, and Challenges for Resourcing Future Generations, *Nat. Resour. Res.*, 2018, **27**(2), 201–216, DOI: 10.1007/S11053-017-9336-5/METRICS.

24 I. González-Álvarez, F. Stoppa, X. Y. Yang and A. Porwal, Introduction to the special Issue, insights on carbonatites and their mineral exploration approach: A challenge towards resourcing critical metals, *Ore Geol. Rev.*, 2021, **133**, 104073, DOI: 10.1016/J.OREGEOREV.2021.104073.

25 N. Dushyantha, N. Batapola, I. M. S. K. Ilankoon, *et al.*, The story of rare earth elements (REEs): Occurrences, global distribution, genesis, geology, mineralogy and global production, *Ore Geol. Rev.*, 2020, **122**, 103521, DOI: 10.1016/J.OREGEOREV.2020.103521.

26 E. O. Opare, E. Struhs and A. Mirkouei, A comparative state-of-technology review and future directions for rare earth element separation, *Renewable Sustainable Energy Rev.*, 2021, **143**, 110917, DOI: 10.1016/J.RSER.2021.110917.

27 U. S. Geological Survey, *Mineral Commodity Summaries 2021*, 2021, DOI: **10.3133/MCS2021**.

28 Indian Bureau of Mines, Nagpur, accessed December 5, 2024, **https://ibm.gov.in/IBMPortal/pages/Indian_Minerals_Yearbook**.

29 M. Aranha, A. Porwal and I. González-Álvarez, Targeting REE deposits associated with carbonatite and alkaline complexes in northeast India, *Ore Geol. Rev.*, 2022, **148**, 105026, DOI: **10.1016/J.OREGEOREV.2022.105026**.

30 M. Aranha, A. Porwal and I. González-Álvarez, Unsupervised machine learning-based prospectivity analysis of NW and NE India for carbonatite-alkaline complex-related REE deposits, *Geochemistry*, 2024, **84**(2), 126017, DOI: **10.1016/J.CHEMER.2023.126017**.

31 E. C. B. Felipe, K. A. Batista and A. C. Q. Ladeira, Recovery of rare earth elements from acid mine drainage by ion exchange Recovery of rare earth elements from acid mine drainage by ion exchange, *Environ. Technol.*, 2021, **42**(17), 2721–2732, DOI: **10.1080/09593330.2020.1713219**.

32 M. Ahmed, Petrology of oligocene coal, makum coalfield, assam, Northeast India, *Int. J. Coal Geol.*, 1996, **30**(4), 319–325, DOI: **10.1016/0166-5162(95)00051-8**.

33 M. Kumar, M. K. Srivastava, K. Kishor and A. K. Singh, An Assessment of the Environmental Impact of Coal Mining through Acid Mine Drainage and Soil Degradation from Makum Coalfields, Upper Assam, India: A Case Study, *J. Geol. Soc. India*, 2023, **99**(8), 1113–1120, DOI: **10.1007/S12594-023-2437-3/METRICS**.

34 B. K. Misra, Optical properties of some Tertiary coals from northeastern India: their depositional environment and hydrocarbon potential, *Int. J. Coal Geol.*, 1992, **20**(1–2), 115–144, DOI: **10.1016/0166-5162(92)90007-J**.

35 ASTM International, *Standards Worldwide*, accessed December 5, 2024, **https://www.astm.org/**.

36 APHA, *Annual Meeting and Expo — "Creating the Healthiest Nation: Preventing Violence"*, accessed December 5, 2024, **https://www.apha.org/events-and-meetings/apha-calendar/2020/2020-apha-annual-meeting-and-expo**.

37 American Public Health Association, *For Science. For Action. For Health*, accessed December 5, 2024, **https://www.apha.org/**.

38 N. Islam, A. Dihingia, P. Manna, *et al.*, Environmental and toxicological assessment of nanodiamond-like materials derived from carbonaceous aerosols, *Sci. Total Environ.*, 2019, **679**, 209–220, DOI: **10.1016/J.SCITOTENV.2019.04.446**.

39 S. U. Gunathunga, E. J. Gagen, P. N. Evans, P. D. Erskine and G. Southam, Anthropedogenesis in coal mine overburden; the need for a comprehensive, fundamental biogeochemical approach, *Sci. Total Environ.*, 2023, **892**, 164515, DOI: **10.1016/J.SCITOTENV.2023.164515**.

40 S. z. Li, Q. c. Xu, M. Liu, *et al.*, Formation, evolution, reconstruction of black shales and their influence on shale oil and gas resource, *China Geol.*, 2024, **7**(3), 551–585, DOI: **10.31035/CG2024060**.

41 Q. Shi, J. Zhao, J. I. Ruijun, *et al.*, Depositional Environment and Origin of Inertinite-rich Coal in the Ordos Basin, *Acta Geol. Sin. (Engl. Ed.)*, 2024, **98**(4), 1064–1085, DOI: **10.1111/1755-6724.15180**.

42 Y. Yang, C. Zhao, Y. Di and Q. Li, Geological exploration of coal mine burnt rock and waterlogged area boundary based on transient electromagnetic and high-density electrical resistivity, *Sci. Rep.*, 2024, **14**(1), 1–14, DOI: **10.1038/s41598-024-55496-6**.

43 M. Bustillo Revuelta, *Geological Occurrence*, 2024, pp. 53–100, DOI: **10.1007/978-3-031-42961-3_3**.

44 Y. Song, Z. Zhang, Y. Liu, F. Peng and Y. Feng, Enhancement of anaerobic treatment of antibiotic pharmaceutical wastewater through the development of iron-based and carbon-based materials: A critical review, *J. Hazard. Mater.*, 2024, **479**, 135514, DOI: **10.1016/J.JHAZMAT.2024.135514**.

45 M. P. Ketris and Y. E. Yudovich, Estimations of Clarkes for Carbonaceous biolithes: World averages for trace element contents in black shales and coals, *Int. J. Coal Geol.*, 2009, **78**(2), 135–148, DOI: **10.1016/J.COAL.2009.01.002**.

46 J. Zou, D. Liu, H. Tian, T. Li, F. Liu and L. Tan, Anomaly and geochemistry of rare earth elements and yttrium in the late Permian coal from the Moxinpo mine, Chongqing, southwestern China, *Int. J. Coal Sci. Technol.*, 2014, **1**(1), 23–30, DOI: **10.1007/S40789-014-0008-3/FIGURES/5**.

47 C. Yu, W. Huang, B. Jiu and R. Hao, Geochemistry Characteristics and Paleoenvironmental Significance of Trace Elements in Coal and Coal Gangue in the Yangcheng Mining Area, Qinshui Basin, *ACS Omega*, 2022, 7(16), 13557–13576, DOI: **10.1021/ACSOMEGA.1C06935/ASSET/IMAGES/LARGE/AO1C06935_0016.JPEG**.

48 C. Yu, N. Mu, W. Huang, W. Xu and X. Feng, Major and Rare Earth Element Characteristics of Late Paleozoic Coal in the Southeastern Qinshui Basin: Implications for Depositional Environments and Provenance, *ACS Omega*, 2022, 7(35), 30856–30878, DOI: **10.1021/ACSOMEGA.2C02596/ASSET/IMAGES/LARGE/AO2C02596_0017.JPEG**.

49 S. Rabha, J. Saikia, K. S. V. Subramanyam, *et al.*, Geochemistry and Nanomineralogy of Feed Coals and Their Coal Combustion Residues from Two Different Coal-Based Industries in Northeast India, *Energy Fuels*, 2018, **32**(3), 3697–3708, DOI: **10.1021/ACS.ENERGYFUELS.7B03907/ASSET/IMAGES/LARGE/EF-2017-03907H_0012.JPEG**.

50 B. K. Saikia, J. Saikia, S. Rabha, L. F. O. Silva and R. Finkelman, Ambient nanoparticles/nanominerals and hazardous elements from coal combustion activity: Implications on energy challenges and health hazards, *Geosci. Front.*, 2018, **9**(3), 863–875, DOI: **10.1016/J.GSF.2017.11.013**.

51 F. Cheng, Y. Zhang, G. Zhang, K. Zhang, J. Wu and D. Zhang, Eliminating environmental impact of coal mining wastes and coal processing by-products by high temperature oxy-fuel CFB combustion for clean power Generation: A review, *Fuel*, 2024, **373**, 132341, DOI: **10.1016/J.FUEL.2024.132341**.

52 W. H. Orem and R. B. Finkelman, Coal Formation and Geochemistry, *Treatise Geochem.*, 2003, **7–9**, 191–222, DOI: **10.1016/B0-08-043751-6/07097-3**.

53 V. V. Seredin and S. Dai, Coal deposits as potential alternative sources for lanthanides and yttrium, *Int. J. Coal Geol.*, 2012, **94**, 67–93, DOI: **10.1016/J.COAL.2011.11.001**.

54 R. Tostevin, G. A. Shields, G. M. Tarbuck, T. He, M. O. Clarkson and R. A. Wood, Effective use of cerium anomalies as a redox proxy in carbonate-dominated marine settings, *Chem. Geol.*, 2016, **438**, 146–162, DOI: **10.1016/J.CHEMGEO.2016.06.027**.

55 M. A. Loader, J. J. Wilkinson and R. N. Armstrong, The effect of titanite crystallisation on Eu and Ce anomalies in zircon and its implications for the assessment of porphyry Cu deposit fertility, *Earth Planet. Sci. Lett.*, 2017, **472**, 107–119, DOI: **10.1016/j.epsl.2017.05.010**.

56 N. D. MacRae, H. W. Nesbitt and B. I. Kronberg, Development of a positive Eu anomaly during diagenesis, *Earth Planet. Sci. Lett.*, 1992, **109**(3–4), 585–591, DOI: **10.1016/0012-821X(92)90116-D**.

57 S. Kumar, A. K. S. Choudhary, A. K. Krishna and S. Maity, Mineralogical variations and geochemical distribution of rare earths and Yttrium (REY) in coal and overburden rocks of some Indian coal mines of Gondwana coalfield, *J. Earth Syst. Sci.*, 2023, **132**(3), 1–22, DOI: **10.1007/S12040-023-02141-X/METRICS**.

58 G. Cornelis, B. Ryan, M. J. McLaughlin, J. K. Kirby, D. Beak and D. Chittleborough, Solubility and batch retention of CeO_2 nanoparticles in soils, *Environ. Sci. Technol.*, 2011, **45**(7), 2777–2782, DOI: **10.1021/ES103769K**.

59 X. Wang, B. Li, M. Zhu, et al., Geochemical behavior of rare earth elements in mining-affected waters, southwest China, *Sci. Total Environ.*, 2024, **957**, 177747, DOI: **10.1016/J.SCITOTENV.2024.177747**.

60 K. Zhang and G. A. Shields, Early diagenetic mobilization of rare earth elements and implications for the Ce anomaly as a redox proxy, *Chem. Geol.*, 2023, **635**, 121619, DOI: **10.1016/J.CHEMGEO.2023.121619**.

61 K. Zhang and G. A. Shields, Sedimentary Ce anomalies: Secular change and implications for paleoenvironmental evolution, *Earth-Sci. Rev.*, 2022, **229**, 104015, DOI: **10.1016/J.EARSCIREV.2022.104015**.

62 M. R. Warke, H. Strauss and S. Schröder, Positive cerium anomalies imply pre-GOE redox stratification and manganese oxidation in Paleoproterozoic shallow marine environments, *Precambrian Res.*, 2020, **344**, 105767, DOI: **10.1016/J.PRECAMRES.2020.105767**.

63 D. Kraemer, N. Tepe, O. Pourret and M. Bau, Negative cerium anomalies in manganese (hydr)oxide precipitates due to cerium oxidation in the presence of dissolved siderophores, *Geochim. Cosmochim. Acta*, 2017, **196**, 197–208, DOI: **10.1016/J.GCA.2016.09.018**.

64 G. Ratié, K. Zhang, M. Iqbal, D. Vantelon, F. Mahé, C. Rivard, M. Komárek, M. Bouhnik-Le Coz, A. Dia, K. Hanna, M. Davranche and R. Marsac, Driving forces of Ce(III) oxidation to Ce(IV) onto goethite, *Chem. Geol.*, 2023, **633**, 121547, DOI: **10.1016/J.CHEMGEO.2023.121547**.

65 H. G. Dill, Can REE patterns and U-Th variations be used as a tool to determine the origin of apatite in clastic rocks?, *Sediment. Geol.*, 1994, **92**(3–4), 175–196, DOI: **10.1016/0037-0738(94)90105-8**.

66 M. Seto and T. Akagi, Chemical condition for the appearance of a negative Ce anomaly in stream waters and groundwaters, *Geochem. J.*, 2008, **42**(4), 371–380, DOI: **10.2343/GEOCHEMJ.42.371**.

67 G. Sun, Y. Wang, Y. Jiang, S. Pan, S. Zhang and M. Zhang, Provenance and tectonic setting of Paleogene sandstone in the center of the northern Qaidam Basin, China, *J. Nat. Gas Geosci.*, 2020, **5**(5), 273–284, DOI: **10.1016/J.JNGGS.2020.09.002**.

68 D. Fathy, M. Wagreich and M. Sami, Geochemical Evidence for Photic Zone Euxinia During Greenhouse Climate in the Tethys Sea, Egypt, *Adv. Sci. Technol. Innov.*, 2022, 373–374, DOI: **10.1007/978-3-030-73026-0_85**.

69 L. Wen, W. Huang, Y. Zhang, J. Bo, Y. Deyu, H. Ruilin and H. Huidi, Mineralogy and Geochemistry of Rare Earth Elements in Carboniferous-Permian Coals at the Eastern Margin of the Ordos Basin, *ACS Omega*, 2024, **9**(30), 32481–32501, DOI: **10.1021/ACSOMEGA.4C00546/ASSET/IMAGES/LARGE/AO4C00546_0016.JPEG**.

70 C. Sethi, B. Hazra, M. Ostadhassan, et al., Depositional environmental controls on mechanical stratigraphy of Barakar Shales in Rajmahal Basin, India, *Int. J. Coal Geol.*, 2024, **285**, 104477, DOI: **10.1016/J.COAL.2024.104477**.

71 J. Li, M. Huang, M. Yu, et al., Provenance and sedimentary environment of REY-rich sediments from the Wharton Basin, Indian Ocean, *J. Asian Earth Sci.*, 2024, **263**, 105996, DOI: **10.1016/J.JSEAES.2023.105996**.

72 S. R. Taylor and S. M. McLennan, The continental crust: its composition and evolution, *Geol. Mag.*, 1985, **122**(6), 673–674, DOI: **10.1017/S0016756800032167**.

73 E. Anders and N. Grevesse, Abundances of the elements: meteoritic and solar, *Geochim. Cosmochim. Acta*, 1989, **53**(1), 197–214, DOI: **10.1016/0016-7037(89)90286-X**.

74 Z. Bao and Z. Zhao, Geochemistry of mineralization with exchangeable REY in the weathering crusts of granitic rocks in South China, *Ore Geol. Rev.*, 2008, **33**(3–4), 519–535, DOI: **10.1016/J.OREGEOREV.2007.03.005**.

75 V. V. Seredin, Rare earth element-bearing coals from the Russian Far East deposits, *Int. J. Coal Geol.*, 1996, **30**(1–2), 101–129, DOI: **10.1016/0166-5162(95)00039-9**.

76 A. Singh, B. P. Singh, S. Kanhaiya, M. A. Quasim, A. Patra, S. Singh and V. K. Srivastava, Geochemistry of Palaeoproterozoic Kajrahat Limestone, Vindhyan Supergroup, central India: insights into depositional conditions and sources of rare earth elements, *Carbonates Evaporites*, 2024, **39**, 30, DOI: **10.1007/s13146-024-00938-5**.

77 C. Chang, F. Li, C. Liu, J. Gao, H. Tong and M. Chen, Fractionation characteristics of rare earth elements (REEs) linked with secondary Fe, Mn, and Al minerals in soils, *Acta Geochim.*, 2016, **35**(4), 329–339, DOI: **10.1007/S11631-016-0119-1**.

78 Y. Kato, T. Kano and K. Kunugiza, Negative Ce anomaly in the Indian banded iron formations: Evidence for the emergence of oxygenated deep-sea at 2.9-2.7 Ga, *Resour.*

Geol., 2002, **52**(2), 101–110, DOI: **10.1111/J.1751-3928.2002.TB00123.X**.

79 B. K. Saikia, A. Saikia, R. Choudhury, P. Xie, J. Liu, T. Das and H. P. Dekaboruah, Elemental geochemistry and mineralogy of coals and associated coal mine overburden from Makum coalfield (Northeast India), *Environ. Earth Sci.*, 2016, **75**(8), 660, DOI: **10.1007/S12665-016-5484-X**.

80 J. Moulder, W. Stickle, P. Sobol and K. Bomben, *Handbook of Standard Spectra for Identification and Interpretation of XPS Data*, Perkin-Elmer Corporation, 1992, vol. 260, accessed September 21, 2024, **https://search.worldcat.org/title/1123943773**.

81 J. F. Moulder, W. F. Stickle, P. E. Sobol and K. D. Bomben, *Handbook of X-Ray Photoelectron Spectroscopy*, Perkin-Elmer, Eden Prairie, MN, 2002, vol. 128, accessed September 21, 2024, **https://books.google.com/books/about/Handbook_of_X_ray_Photoelectron_Spectros.html?id=A_XGQgAACAAJ**.